AIAA AVIATION Forum
June 15-19, 2020, VIRTUAL EVENT
AIAA AVIATION 2020 FORUM

10.2514/6.2020-2819

Preliminary Investigation of Jitter Induced by the Atmosphere on Laser Beam Propagation from an Airborne Platform

Matthew T. Kalensky[1], Eric J. Jumper[2], and Stanislav Gordeyev[3]

University of Notre Dame, Notre Dame, IN, 46556

This paper describes a preliminary investigation of predicting jitter of the laser beam at the target when projected from an airborne platform moving through the turbulent atmosphere. The beam jitter is computed by propagating a laser beam through a Kolmogorov simulated atmosphere for various C_n^2 values over a 5 [km] range, directed from the platform at 90º off the flight direction. The significance of this study over previous approaches is that actual tracking scenarios are replicated and the results are compared with the literature. It was found that the jitter imposed by the atmosphere is significant and low bandwidth compensation rates in adaptive optics system components such as fast steering mirrors, can make the resultant "corrected" signal worse. The results place new tracking performance limitations on airborne laser systems.

Keywords: atmospheric turbulence, jitter, airborne laser systems, beam control.

Nomenclature

C_n^2	= Index of refraction structure constant
D_n	= Index of refraction structure function
f_C	= Compensation/corrective frequency
f_{TG}	= Tyler/tracking frequency (G-tilt definition)
f_{TZ}	= Tyler/tracking frequency (Z-tilt definition)
L	= Range
U	= Velocity
λ	= Wavelength
κ	= Wavenumber
ψ	= Wave field
Ψ	= Two-dimensional Fourier transform of ψ
θ	= Phase field
ρ	= Two-dimensional position vector
n	= Index of refraction
δ_x	= Phase screen thickness
Φ	= Energy spectrum
ϕ	= Wave field
A	= Amplitude
σ_x	= Streamwise jitter
σ_y	= Spanwise jitter

[1] Graduate Research Assistant, Department of Aerospace and Mech. Eng., Student AIAA Member
[2] Professor, Department of Aerospace and Mech. Eng., AIAA Fellow
[3] Associate Professor, Department of Aerospace and Mech. Eng., AIAA Associate Fellow

σ_Z = Theoretical jitter (Z-tilt definition)
σ_G = Theoretical jitter (G-tilt definition)
r = Separation in structure function
D = Aperture Diameter
WF = Wavefront
OPD_{RMS} = Optical Path Difference
r_0 = Fried parameter

I. Introduction

Propagation of laser beams through the atmosphere is relevant to optical communication, imaging, and directed energy systems [1,2,3,4]. The statistically random fluctuations of refractive index in the atmospheric medium are deleterious to the functionality and operation of these systems [1]. One of the functions of a beam control system is to track and maintain aim point on the target, to jitter values less than λ/D, where λ is the laser wavelength and D is the laser beam diameter or aperture at the exit pupil. Other researchers [see 5, for example] have recognized that motion through the turbulent atmosphere imposes jitter, or bulk angular motion, on the laser beam. The atmosphere is comprised of turbulent structures ranging in size from hundreds of meters down to millimeters. The large-scale structures of the atmosphere, generated by wind shear and thermal plumes, produce vortical structures referred to as the outer scales. At the smallest scales of turbulence, energy is dissipated through the action of viscosity. Between the largest and smallest scales is an inertial subrange where turbulence is considered isotropic and Kolmogorov's theory applies. It has been shown that the Kolmogorov velocity perturbations are related to density variations, which consequently, linearly induce index of refraction fluctuations through the Gladstone-Dale relation. These variations are quantified by the index-of-refraction structure function, C_n^2. In general, the unsteadiness in the atmosphere is slow. However, in the presence of wind, the temporal variation is not stationary and is usually quantified by the Greenwood frequency [6]. More importantly, the speed of an aircraft passing these large-scale structures imposes unsteady jitter on the beam which is dependent on the aircraft speed. This contribution to laser beam jitter imposes certain requirements and limitations on the tracking and aim-point maintenance functions of the beam control system. The problem of atmospheric induced jitter has been treated analytically in Ref. [5]. However, the behavior and response of actual hardware operations in airborne tracking systems has not been examined as it is here, laying the groundwork for future experimental measurements of this phenomena.

A. Description of Tip/Tilt Induced Effects

Imposing a finite sized aperture to view optical distortions with a wide range of spatial frequencies acts as a form of a spatial filter [7]. Consequently, this spatial filter imposes requirements and defines challenges with development of an adaptive optics system and the associated components. If a beam is propagated through turbulent structures larger than the size of the viewing aperture, the resultant beam will see a net deflection, known as tip/tilt. This net deflection of the beam varies in time. In the near-field, tip/tilt is just a linear shift in phase of the wavefront. However, in the far-field, tip/tilt changes the location of where the beam strikes the target [7]. Low frequency tip/tilt changes or slowly varying net beam deflection is colloquially referred to as "drift." Due to the low frequency nature, this drift is often relatively easy to correct for in a typical adaptive optics configuration. Conversely, high frequency changes in tip/tilt, referred to as "jitter," are more detrimental and harder to correct [8]. Jitter alters the direction, not the shape of the outgoing beam. Therefore, the Strehl Ratio (SR) is unaffected by tip/tilt when referenced to the center of the beam. Despite not affecting the SR, jitter is deleterious to laser system performance since the high frequency movement of the beam does not allow a concentrated amount of energy to be held on the target [7]. Additionally, when measuring the distortions imposed on a wavefront using devices such as a Shack Hartmann Wavefront Sensor (WFS), the tip/tilt resultant from optical turbulence is typically removed from experimental data because it is difficult to decouple from the jitter associated with mechanical contamination. The coupling of these issues makes jitter difficult for adaptive optics systems to compensate for.

B. Turbulence Parameters

In order to simulate beam propagation through an atmospheric medium, the physics and dynamics of the turbulent atmosphere need to be understood. Full understanding of the spatial and temporal characteristics of the atmosphere would require solving the non-linear Navier Stokes equations. Therefore, Kolmorogov suggested a theory that was statistically motivated and is centered around the idea of an energy cascade, where "energy" is injected at the largest scales and cascades down via inertial forces through smaller and smaller scales until eventually the remaining energy is dissipated as heat [9,10,11]. In the intermediate region, referred to as the inertial subrange, the energy at each scale is a function of structure size only. Obukhov built on the work of Kolmorogov and showed that in the atmosphere, temperature can be modeled as a conservative passive scalar and therefore, using a similar procedure as Kolmogorov, arrived at an energy spectrum for temperature [12,14]. Much of the atmospherics community today still refers to the text of Tatarskii as he applied his predecessor's theoretical constructs to wave propagation in turbulence [13]. Using the findings established by Kolmogorov and Tatarskii, additional useful turbulence parameters have since been derived. One of these parameters is the Fried coherence length or parameter, r_0. The Fried parameter is qualitatively defined as the maximum size aperture that can be used before atmospheric imposed aberrations *significantly* limit system performance [8]. For environments of constant C_n^2, the Fried coherence length for plane waves is described by Eq. 1. For spherical waves and constant C_n^2 along the propagation path, the Fried coherence length can be described by Eq. 2 [8, 15]. Here, L is the range and κ is the wavenumber.

$$r_0 = 1.68(C_n^2 L\kappa^2)^{-3/5} \tag{1}$$

$$r_0 = 3.0(C_n^2 L\kappa^2)^{-3/5} \tag{2}$$

Another parameter of interest to this study is the Tyler frequency, f_T. Tyler recognized that a transfer function can be derived which describes the response of a tilt-tracking servo [5]. The utility of the fundamental tracking frequency, or Tyler frequency, f_T, is such that if f_T equals the tilt-tracking hardware bandwidth, f_C, the rms one axis jitter is equal to λ/D, as seen in Eq. 3 [5]. Tracking frequencies, as derived by Tyler, for both gradient tilt (G-tilt) and Zernike tilt (Z-tilt) are presented in Eqs. 4 and 5, respectively [5,8]. Additionally, Eqs. 6 and 7 allow for calculation of jitter if uncorrected, for both G-tilt and Z-tilt definitions, respectively.

$$\sigma = \left(\frac{f_T}{f_C}\right)\left(\frac{\lambda}{D}\right) \tag{3}$$

$$f_{T_G} = 0.331 D^{-1/6}\lambda^{-1}\left[\int_0^L C_n^2(z)U^2(z)dz\right]^2 \tag{4}$$

$$f_{T_Z} = 0.368 D^{-1/6}\lambda^{-1}\left[\int_0^L C_n^2(z)U^2(z)dz\right]^2 \tag{5}$$

$$\sigma_G^2 = 0.170\left(\frac{\lambda}{D}\right)^2\left(\frac{D}{r_0}\right)^{5/3} \tag{6}$$

$$\sigma_Z^2 = 0.182\left(\frac{\lambda}{D}\right)^2\left(\frac{D}{r_0}\right)^{5/3} \tag{7}$$

C. Adaptive Optics System

The field of adaptive optics is concerned with compensating for aberrations imposed on a laser beam in order to improve the quality of the resultant wavefront for a specific application. Adaptive optics methods have been studied for astronomical purposes in order to reduce image blurring associated with seeing distant stars. In the field of directed energy, adaptive optics is concerned with correcting phase distortions (by applying a phase conjugate) in order to limit intensity losses on a far-field target [8]. For diffraction limited propagation, the far-field power-in-the-bucket values are inversely proportional to the square of λ/*D* where λ is the laser wavelength and *D* is the aperture diameter [16]. The phase distortions imposed on the laser beam arise from different physical mechanisms. The aerodynamic turbulence around a high-speed moving platform imposes high frequency, small scale spatially and temporally evolving structures. The atmospheric turbulence encountered with long

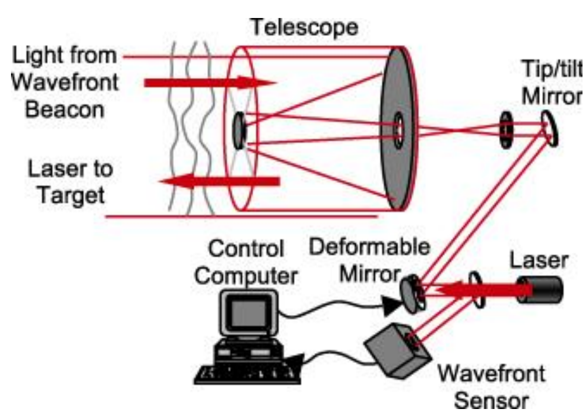

Figure 1. Example adaptive optics system, from [17].

propagation distances has associated large scale turbulence structures and the intensity of which depends on the environment, namely C_n^2. Adaptive optics systems need to be robust to compensate for the range of frequencies distorting the beam. As mentioned before, the aperture acts as a form of spatial filter in which structures larger than the size of the viewing aperture cause a tip/tilt in the resultant wavefronts and smaller scale, high frequency structures smaller than the aperture size become higher order effects. These various types of aberrations are compensated for differently in an adaptive optics system. For the purposes of the work presented here, a "typical" adaptive optics systems configuration will be referred to for explanatory purposes. Typical configurations consist of light from a distant image or beacon source entering the system, which usually consists of a telescope, fast steering mirror (FSM) or tip/tilt mirror, a deformable mirror (DM), and a WFS as illustrated in Fig. 1. The wavefront sensor coupled with a CCD camera enables the distortions on the incoming beam to be measured and quantified. This information is relayed along to a control algorithm. The control algorithm uses the information received from the WFS to send signals to other system components such as the DM and FSM [18]. This procedure is performed in a closed loop operation. Figure 1 illustrates an example adaptive optics system which uses a laser to project a beam back out through the system. Since the laser is striking the same corrective optics, the outgoing beam will have an altered wavefront indicative of the distortions registered on the incoming wavefront from the light beacon. Therefore, the laser's wavefront at the far-field target will ideally have limited distortions, assuming the outgoing and incoming beam propagate across similar paths.

The work here is concerned with the distortions imposed by propagating past large scale atmospheric turbulent structures. These types of aberrations will exist as jitter and therefore, require tip/tilt correction. Tip/tilt, which is an unsteady pointing of the beam, can be corrected for by using a FSM. FSMs apply correction on two axes' by angling the mirror to compensate for the measured tilt and to re-center the pattern in the far-field. Jitter is a function of aperture size, turbulence intensity, and speed of passing turbulent structures. These parameters are ultimately what decide the tracking requirements necessary for this correction in an adaptive optics system.

II. Modeling

The work discussed here seeks to computationally quantify the aberrations imposed on an originally unperturbed light source as the beam propagates through a simulated atmosphere from a moving platform. In order to do this, the well-known phase screen approach is used to replicate the atmospheric environment. A propagation algorithm is then employed which uses Fourier optics to predict the behavior of the beam as it is projected through each phase screen. The far-field beam pattern is analyzed, and the global tip/tilt values are computed, enabling requirements necessary for correction to be further studied. Greater detail for each of these steps will be discussed in the sections to come.

A. Phase Screen Generation

Using phase screens to simulate the atmosphere is a common practice [19,20,21]. The wave field is defined such that it satisfies the parabolic approximation to the wave equation; enabling the atmosphere to be treated as "slices" with a certain thickness. The wave field and parabolic approximation to the wave equation are shown in Eqs. 8 and 9, respectively [19]. Here, each slice of atmosphere will impose pseudorandom phase variations onto a laser beam projected through it but with little change in amplitude. Using Gaussian white noise, random amplitude and phase matrices are generated and multiplied by a given spectrum. Since this study pertains to propagation through the atmosphere, the von Kármán power spectrum is used and shown in Eq. 10 [21]. Taking the two-dimensional inverse Fourier transform of this result yields a phase screen of thickness, δ_x, with amplitude and phase corresponding to the well-accepted atmospheric model. This procedure is repeated for as many phase screens as needed. Since this study involves propagation on a moving platform, a defined velocity component is incorporated into each phase screen. An example phase screen is shown in Fig. 2.

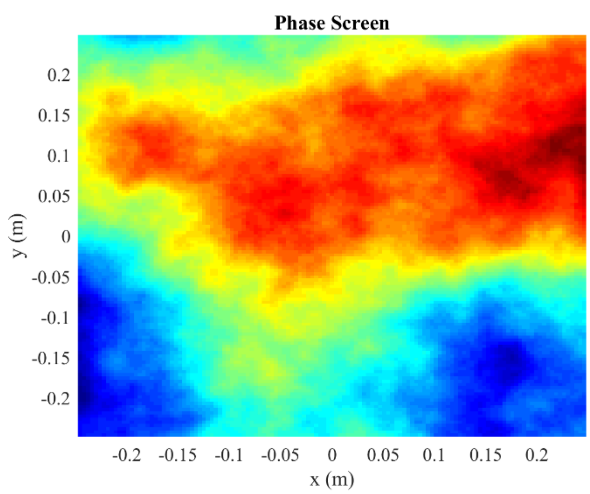

Figure 2. Example phase screen.

$$\phi = \psi \exp(-ikx) \tag{8}$$

$$2ik\frac{\partial\psi}{\partial x} + \left(\partial_{yy} + \partial_{zz}\right)\psi + 2k^2(n - \langle n\rangle)\psi = 0 \tag{9}$$

$$\Phi_n(\kappa) = \frac{0.033C_n^2}{(\kappa^2 + \kappa_0^2)^{11/6}} \tag{10}$$

B. Propagation Algorithm

Once phase screens that are statistically representative of the atmosphere are generated, a propagation algorithm needs to be used in order to simulate the behavior of a beam propagating through these screens. We define, $\Psi(x,\boldsymbol{\kappa})$ as the two-dimensional Fourier transform of $\psi(x,y,z)$. From here, if the fluctuations of refractive index are assumed to be zero between phase screens, the Fourier transform of the wave equation shown in Eq. 11, is described as follows. This equation has a solution in the form shown in Eq. 12 [19].

$$\frac{\partial\Psi(x,\kappa)}{\partial x} = -i\frac{\kappa^2}{2\kappa}\Psi(x,\kappa) \tag{11}$$

$$\Psi(x_2,\kappa) = \Psi(x_1,\kappa)exp\left[-i\frac{\kappa^2(x_2 - x_1)}{2\kappa}\right] \tag{12}$$

These equations allow the beam to be projected from screen to screen. The steps are as follows. First, x_1 is treated as the location of wave field for the beam at the start of the first phase screen. x_1 describes the beam after traversing the first phase screen but before entering the next phase screen. The wave field at the beginning of the phase screen is described by Eq. 13, where the ψ term represents the amplitude field and the exponential term represents the phase field for that particular screen. Next, Eq. 13 is transformed to convert into spectral space and this result is plugged into Eq. 14, which is the solution of the Fourier transformed wave equation, the result of which is seen in Eq 12. Using an inverse Fourier transform, the result from Eq. 14, is converted back into the spatial domain. This result now represents the wave field for the beam at the end of the phase screen and will be used as the initial conditions for the beginning of the next phase screen. This procedure is repeated until the final phase screen is traversed [19]. The procedure of stepping through each phase screen is visually represented in Fig. 3.

$$\psi(x_1,\boldsymbol{\rho}) = \psi(x_1-,\boldsymbol{\rho})\ \exp\ (i\boldsymbol{\theta}(\boldsymbol{\rho})) \tag{13}$$

$$\Psi(x_2-,\boldsymbol{\kappa}) = \Psi(x_1,\boldsymbol{\kappa})exp\left[-i\frac{\boldsymbol{\kappa}^2(x_2 - x_1)}{2\boldsymbol{\kappa}}\right] \tag{14}$$

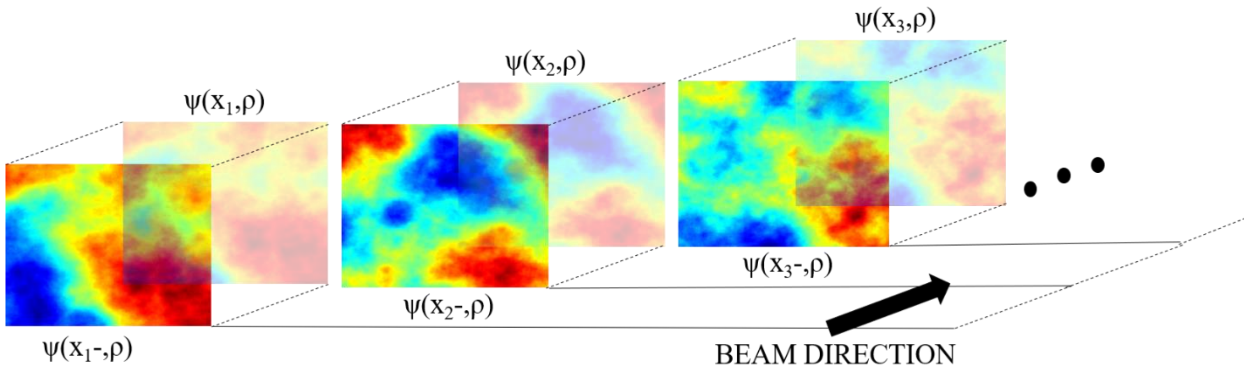

Figure 3. Propagation algorithm procedure.

C. Collimated versus Uncollimated Beams

In this study, simulations are performed with beams which are both collimated as well as uncollimated; or the beam is focused onto a target. Collimated beam propagation simplifies studying residual jitter however a focused beam represents the scenario more realistic to applications. The algorithm is altered to accommodate focusing the beam to a point across the propagation range by multiplying an exponential term to the initial beam profile [22].

D. Jitter Extraction Methods

After the beam has been propagated through the phase screens using the procedure described above, jitter is extracted from the resultant far-field beam pattern. When measuring tip/tilt, there are two definitions prevalent in literature: gradient tilt (G-tilt) and Zernike tilt (Z-tilt). G-tilt is the result of averaging all local gradients over a wavefront. Z-tilt comes from the first radial degree terms of the Zernike polynomial expansion.

Tip, tilt, and piston represent the three lowest order Zernike modes. In order to calculate Z-tilt, a least squares fit is applied to the plane of the wavefront. The error associated with the least squares fit of the wavefront plane is minimized by solving a system of linear equations and the resultant coefficients A, B, and C, are the tip, tilt, and piston values respectively [7,23]. The equation for error can be seen in Eq. 15. Here, the tip, tilt coefficients as a function of time are the "global" tilt, as opposed to "local" tilt. Local tilt will not be used in this work. For the case of collimated beam propagation, jitter is extracted using this Z-tilt definition of jitter. This procedure is performed on the far-field apertured beam.

$$\mathrm{Error(A,B,C)} = \iint_{Ap} (WF(x,y,t) - [A(t)x + B(t)y + C(t)])^2 \, dxdy \tag{15}$$

For the case of the uncollimated focused beam, jitter cannot be extracted with the procedure described above. Unlike the collimated beam where the far-field pattern is the size of the receiving aperture, the far-field energy pattern for this case is focused to nominally a point. However, diffraction and higher order distortion effects serve to spread energy away from the projected center of the far-field focused beam. This scenario constitutes using a centroiding method to extract jitter from the far-field beam as shown in Eq. 16, where A is the amplitude of the light. In the absence of jitter, the highest energy will land at the location where the beam was aimed in the far-field, $(x,y)=(0,0)$. By calculating a centroid based on the beam intensity at the receiving plane of the simulated propagation path, x and y jitter can be calculated using the physical far-field beam displacement.

$$\sigma_x(t) = \frac{\sum A_i x_i}{\sum x_i} \text{ and } \sigma_y(t) = \frac{\sum A_i y_i}{\sum y_i} \tag{16}$$

E. Tip/Tilt Correction Methods

Once the propagation algorithm is used, the far-field beam can be analyzed. The work here is particularly interested in the jitter imposed on the beam resultant from traversing the atmosphere. Therefore, the far-field beam is computationally apertured and the associated global tilt is calculated for each scenario. For compensation in an adaptive optics system, tip/tilt angles are extracted from CCD imagery, and a correction signal is sent to system hardware (FSM). The work discussed below will model the bandwidth necessary for compensation given a set of situational parameters.

E.1 Fourier Approach

The simplest compensation approach is to treat the correction hardware as a high pass filter. For each apparatus, there exists a limit on the speed for which the hardware can be driven to fix the aberrated beam. Therefore, as a preliminary gauge, it is reasonable to impose a high pass filter such that all frequencies below the cutoff are capable of being corrected (Jitter,$\sigma=0$), and all frequencies above the cutoff remain uncompensated for. It is expected that this procedure represents the least conservative predictive approach, meaning that this method likely overpredicts the success of the correction.

E.2 Instantaneous Correction

The instantaneous correction method more appropriately mimics the correction sequence seen in an adaptive optics system. Let's assume that the incoming beam is sampled fast enough such that all jitter information is represented in the data. As previously mentioned, there exists a limit on the bandwidth for which a system can correct. For this case, assume a correction is applied at a discrete point in time using hardware such as a FSM. At this instant in time, the tilt value is set to $\sigma=0$ µrad. In the time between when the first correction and the next correction takes place, high frequency jitter may exist which goes uncorrected for. This type of approach clearly defines a speed which a corrective measure needs to be applied in order to mitigate jitter to within a desired quantity. This type of compensation approach is illustrated in Fig. 4 for two correction points indicated by red circles. In the Fig. 4 left plot, the red circle represents the first-time instance where a correction is applied. It can be seen that at that point, the jitter amplitude is brought to 0 µrad and the entire subsequent signal is offset by that same amount. Fig. 4 right plot indicates where the second correction occurs. Again, the red circle indicates the correction point and at this time location, the jitter amplitude is brought to zero. Although these figures are for visualization purposes, it is clear that jitter still exists between the two correction points, the same way jitter exists between correction points using a FSM or tilt mirror in an adaptive optics application. Therefore, there is a correction speed that will mitigate the jitter signal to within a desired amplitude; usually regarded as λ/D. There exists a worse scenario where very slow compensation rates could potentially make the "corrected" signal, worse than the raw jitter time series.

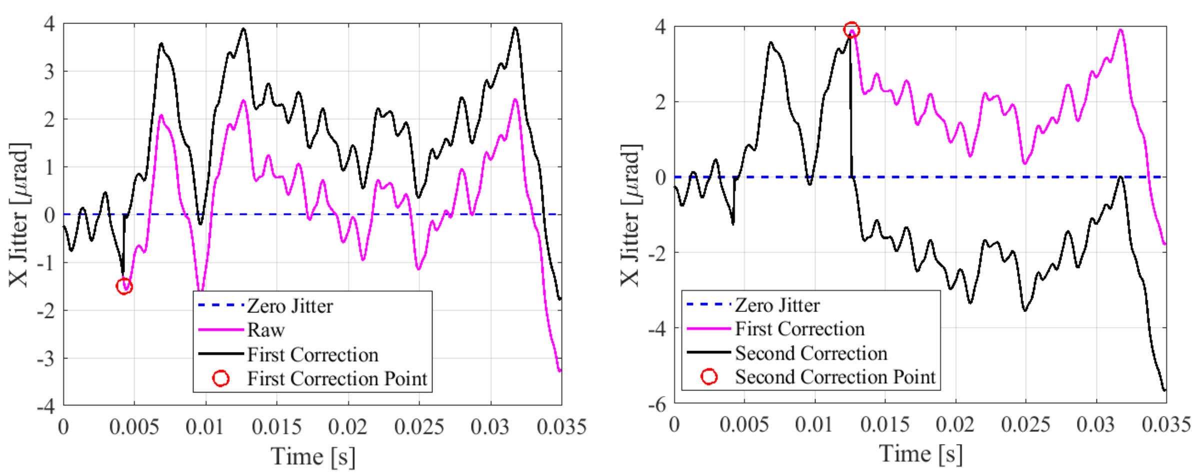

Figure 4. Left) First correction using the instantaneous approach. Right) Second correction using the instantaneous approach.

E.3 Correction using an Exposure Time

The difference between this section and the previous is that now, instead of making an instantaneous correction, the correction is based on previous information with a simulated exposure time. The instantaneous correction cases described above represent an idealized scenario. In actuality, there will always be an exposure time associated with the CCD acquisition as well as an overall system latency. This exposure/latency effect acts as the time necessary for adaptive optics systems to read in data, calculate a correction, and send a corrective signal to the system hardware to actually implement a fix. This effect is replicated here by averaging over a specified time of previous jitter time series data. This value is then used for the correction. It is expected that this type of approach will be the most deleterious to jitter correction as well as most realistic to what is seen in adaptive optics systems. This approach is illustrated in Fig. 5 where the dotted vertical green lines indicate the period of time associated with the simulated exposure.

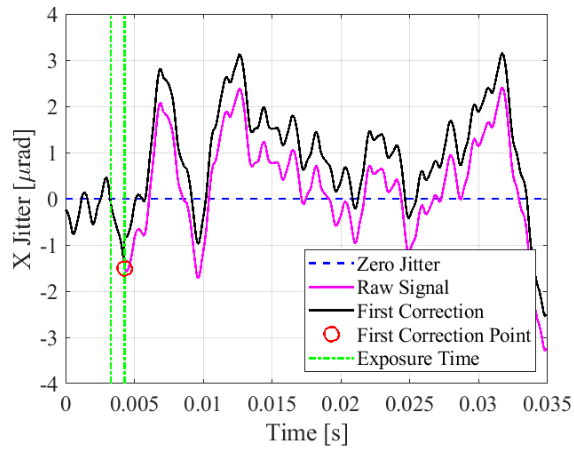

Figure 5. Exposure incorporated approach.

III. Computational Results and Discussion

The simulation results pertaining to the approaches discussed above are presented below. For all simulations, a C_n^2 value of 1e^{-15} [m$^{-2/3}$] and propagation distance of 5 [km] was selected . This value of C_n^2 was selected as previous experimentation (described in great detail in Ref. [24]) as well as literature indicate that this is a relevant turbulence strength for the altitudes of interest. Each phase screen was 256x256 points where *dx* and *dy* were .002 m. Simulated wavefronts were sampled at 5 kHz producing a *dt* between frames of 0.0002 s. 10 phase screens were used for these simulations meaning each screen had a thickness of 500 m. This phase screen thickness also ensured that only weak fluctuations in intensity develop over the distance across the phase screens [20]. For the simulations conducted here, an aperture size of 0.3 [m], a platform convective speed of 264 m/s, and a wavelength of 1 μm were defined. Since Gaussian white noise is used to generate random phase and amplitude matrices, every simulation yields slight variations in compensation results. For this reason, 15 simulations are conducted for each scenario and the results are averaged. Additionally, for the exposure incorporated compensation approach, an exposure time of 0.001 s was used for all cases.

A. Collimated Beam Simulation Results

Figure 6 left plot compares the rms jitter values in the streamwise, x-direction as a function of the correction frequency, f_C, using the Fourier filter, the instantaneous correction, and the exposure incorporated correction approaches. Here the solid black line indicates the uncorrected rms streamwise, x-jitter value and the red dashed line presents the -3dB mark referenced to the uncorrected jitter, where the uncorrected jitter is approximately 3 μrad. The horizontal dashed blue line in the plot is the theoretical jitter prediction calculated using Eq. 7. When comparing the various compensation approaches, as expected, the Fourier filter estimates the lowest residual jitter. The instantaneous correction and the exposure incorporated correction approaches more appropriately mimic the mechanical correction mechanism seen in an adaptive optics system when a FSM is used. For these two approaches, the low frequency compensation rates (200, 400, and 600 Hz) tend to make the streamwise, x-jitter rms worse than, or nominally improved when compared to the uncorrected value. The instantaneous approach tends toward the -3dB compensation mark at a correction frequency of 1200 [Hz] whereas the exposure incorporated approach asymptotes and never reaches the -3dB correction mark over the range of realistically "fixable" correction speeds. Also illustrated in the plot is a dotted blue line with square markers which represents the theoretical system response derived by Tyler (Ref. [5]) and calculated using Eq. 5. Here it can be seen that the fundamental tracking frequency, f_T, tends to overpredict the system's ability to correct jitter at higher compensation rates. Figure 6 right plot presents the rms jitter values in the spanwise, y-direction with the same correction procedures described above. Here, the uncorrected jitter value was approximately 2.9 μrad. Since there is no propagation speed in the spanwise direction, the compensation approaches are more successful at further reducing jitter. Similarly, the theoretical values were not plotted as there was no "wind" or propagation speed present in this direction.

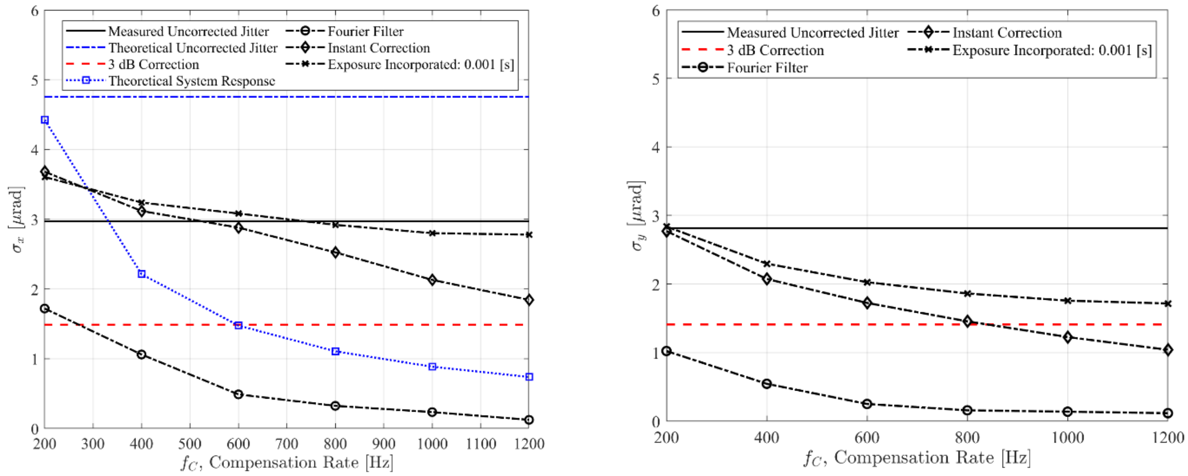

Figure 6. RMS Jitter values for a collimated beam using various compensation approaches.

B. Focused Beam Simulation Results

For this case, the beam is uncollimated to simulate focusing a beam from the aperture to the target. Figure 7 illustrates that the beam is the size of the defined aperture at the beginning of the propagation path and is then focused to a point at the end of the propagation path. Using this focused beam type of engagement, Fig. 8 compares the measured jitter with the residual jitter calculated again using the various compensation approaches discussed above. This simulation also used an aperture size of 0.3 [m], a platform propagation speed of 264 m/s, and a wavelength of 1 µm. Figure 8 left plot illustrates the results for the streamwise, x-direction. The uncorrected x-jitter value for the focused case was approximately 1.7 µrad. Again, the instant correction and exposure incorporated correction methods tend to make jitter worse than, or similar to the original signal for the low compensation rate cases (200, 400, and 600 Hz). Despite marginally improving jitter at higher compensation rates, both methods struggle to improve the jitter signal to the desired -3dB mark. Also presented in the plot are the theoretical uncorrected jitter values as well as the theoretical tilt mirror correction response calculated using Eqs. 4 and 2, respectively. These equations are used since the G-tilt definition is more suitable for the centroid based means of calculating jitter for the case of the focused beam [5].

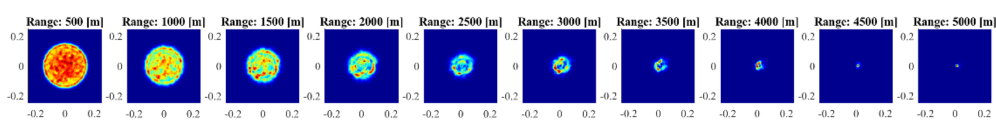

Figure 7. Focused beam at the end of each phase screen.

Figure 8 right plot illustrates the spanwise, y-jitter results. Again, the compensation approaches are more successful at reducing jitter due to no propagation speed in the spanwise direction. Here, the uncorrected rms jitter value is approximately 1.8 µrad.

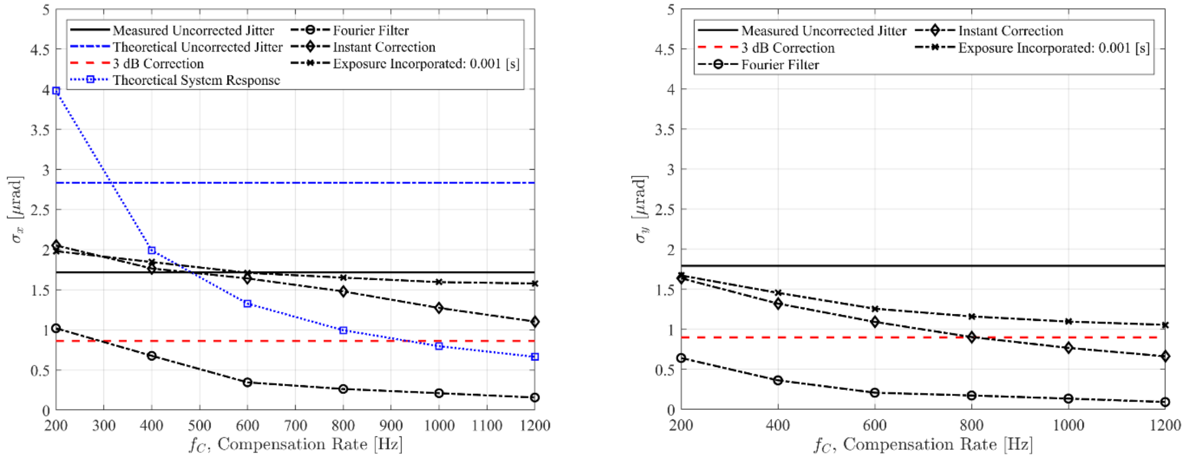

Figure 8. Jitter$_{\mathbf{RMS}}$ values for a focused beam using various compensation approaches.

IV. Ongoing Work

The goal of the work is to ultimately define the requirements for an adaptive optics system's jitter correction, given an input set of environmental scenarios. To this point, the work presented here has inspired the need for experimental validation of these computational simulation results. The Airborne Aero-Optics Laboratory for Beam Control (AAOL-BC) was employed for this purpose.

The primary objective of AAOL-BC is to provide an in-flight testing platform where aero-optics experiments can be performed under realistic conditions [25]. AAOL-BC consists of two Falcon-10 aircrafts capable of flying at varying separations, altitudes, and Mach numbers. One of the aircrafts, designated as the source aircraft, projects a 532 nm diverging laser beam onto a custom-designed optical quality window mounted on the second aircraft, referred to here as the laboratory aircraft. The window is mounted on a specially designed aluminum mount, meant to limit distortions to the attached boundary layer as fluid convects from the aircraft fuselage over the window [25]. For this experiment, the two AAOL-BC aircrafts will fly at large separations in order to measure the jitter imposed by the atmosphere onto the laser beam. Presumably, large separations between aircrafts as well as lower altitude flights will impose more atmospheric contribution. For this reason, the test matrix of this experiment will vary both separation between aircrafts as well as altitude. This experiment demands high bandwidth and robust tracking capability on both aircrafts. The experimental results obtained in these flight campaigns will be used to compare with and validate the computational results seen in this paper. These experimental data and comparisons to computational results are to come.

A. Simulating the Experimental Test Environment

Further simulations were conducted that predict the jitter and wavefront error, or OPDrms, for these experimental campaigns. In these simulations, an aperture of 0.2 [m] was used, matching the size of the aperture on the AAOL-BC laboratory aircraft. The simulations used a Mach number of 0.4 which matches the Mach number for which the experimental aircrafts flew during the flight campaigns. Additionally, a wavelength of 532 nm was used to match the wavelength of the laser installed on the AAOL-BC source aircraft. During experiment, the AAOL-BC aircrafts fly at both varying altitudes and separations. Since preemptively knowing the experimental C_n^2 environment is not feasible, various C_n^2 test cases were simulated. The jitter results from these simulations can be found in Fig. 9.

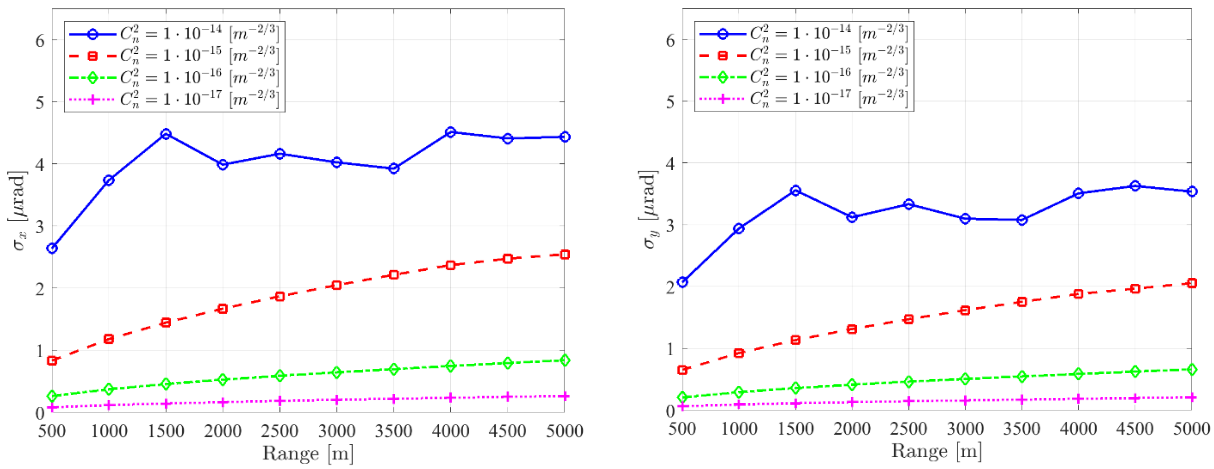

Figure 9. Jitter$_{RMS}$ for simulations matching experimental setup as a function of range for various C_n^2 environments.

For low altitude flights, typical C_n^2 values can be in the range from 1x10^{-15} to 1x10^{-14} [m$^{-2/3}$]. As shown in Fig. 9, data collected at low altitudes may reveal streamwise, x-jitter values from 1 to 4.5 μrad, depending on the separation of the aircrafts (propagation range). Also shown in Fig. 9, is that flying at higher altitudes where the C_n^2 regimes are significantly lower (1x10^{-17} to 1x10^{-15} [m$^{-2/3}$]), imposes significantly less jitter onto the measured laser beam where x-jitter values are now a fraction of a microradian.

Figure. 10 presents the wavefront error, or OPDrms, computed from the simulation described above. OPDrms is the typical metric for quantifying higher order wavefront distortions. Since the atmospheric structures are much larger than the size of the acquisition aperture, the OPDrms corresponding to these simulated results is small. Figure 10 reveals that the wavefront error across the various C_n^2 cases at most approaches a tenth of a micron.

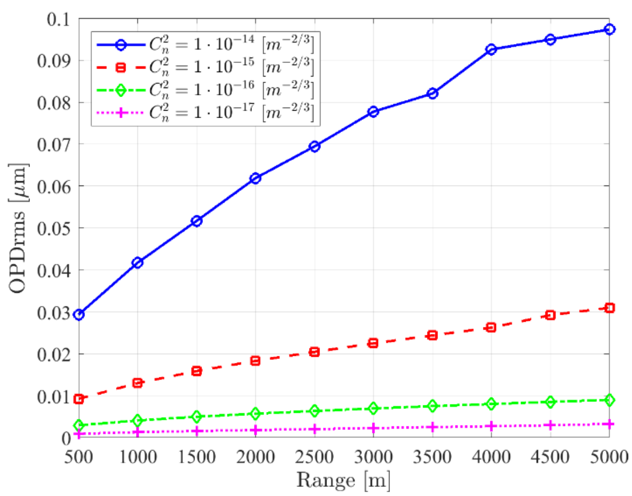

Figure 10. OPD$_{RMS}$ for simulations matching experimental setup as a function of range for various C_n^2 environments.

V. Conclusions

The work presented here has investigated predicting jitter of a laser beam at a target when projected from a moving platform through the atmosphere. The beam jitter is computed by propagating a laser beam through a Kolmogorov simulated atmosphere for various C_n^2 values over a 5 [km] range. Various jitter correction approaches are presented and their compensation results place new tracking performance limitations on airborne laser systems. It was shown that for long range engagements, the simulated atmosphere imposes significant jitter onto the laser beam. When simulating jitter compensation methods, the Fourier correction method and theoretical system response tend to overpredict the success of jitter rejection. Conversely, the instantaneous correction and exposure incorporated correction methods, which are more realistic at modeling adaptive optics system hardware, revealed that insufficient corrective bandwidths up to f_C=600 Hz can tend to make jitter worse or unimproved.

This study has inspired the need for experimental testing using AAOL-BC. Here, the two AAOL-BC aircrafts will fly at large separations as well as lower altitudes. It is expected that significant atmospheric induced jitter will be imposed onto the beam. Further simulations were conducted to match these experimental test conditions. It was found that for ranges up to 5 km between the aircrafts and low altitude flights, up to 4.5 μrad of jitter may be imposed on the laser beam from the atmosphere. These findings will be used to compare with and validate future experimental results.

VI. Acknowledgments

This work is supported by the Joint Technology Office, Grant number FA9550-13-1-0001 and Office of Naval Research, Grant number N00014-18-1-2112. The U.S. Government is authorized to reproduce and distribute reprints for governmental purposes notwithstanding any copyright notation thereon.

VII. References

1. Fitzgerald, E.J. and Jumper, E.J., “The Optical Distortion Mechanism in a Nearly Incompressible Free Shear Layer,” Journal of Fluid Mechanics, 512, pp. 153-189, 2004.
2. Jumper, E.J., Zenk, M., Gordeyev, S., Cavalieri, D., and Whiteley, M., "Airborne Aero-Optics Laboratory”, Journal of Optical Engineering, 52(7), 071408, 2013.
3. Gordeyev S., Jumper E., “Fluid Dynamics and Aero-Optical Environment Around Turrets,” AIAA 2009-4224.
4. Gilbert K.G., Otten L.J., “Aero-Optical Phenomena,” Progress in astronautics and aeronautics series, Vol. 80. New York: American Institute of Aeronautics and Astronautics, 1982.
5. Tyler, G., “Bandwidth consideration for tracking through turbulence,” J. Opt. Soc. Am., Vol. 11, No. 1, Jan., 1994.
6. Greenwood, D.P., ”Bandwidth specification for adaptive optics systems,” J. Opt. Soc. Am., Vol. 67, No. 3, March 1977.
7. Siegenthaler J.P., *Guidelines for Adaptive Optic Correction Based on Aperture Filtration*, University of Notre Dame, PhD dissertation, 2009.
8. Tyson, R.K., *Principles of Adaptive Optics*, Academic Press, 2nd Ed., 1998.
9. Kolmogorov, A.N., “On degeneration of turbulence in incompressible viscous fluid”, C.R. Akad. Sci. SSR (Dokl.) Vol 31(6), 1941, pp 538-541.
10. Kolmogorov, A.N., “The local structure of turbulence in incompressible viscous fluid for very large Reynolds numbers” Dokl. Akad. Nauk SSSR 30, pp 301-305 (1941).
11. Batchelor, G.K., *Homogeneous Turbulence*, Cambridge University Press, Cambridge, 1953.
12. Obukhov, A. M., “Temperature field structure in a turbulent flow,” Izv. AN SSSR (Geogr. and Geophys. series), 13, 58–69 1949.
13. Tatarski, V.I., *Wave Propagation in a Turbulent Medium*, McGraw-Hill, New York, 1961.
14. Siegenthaler, J.P., Jumper, E.J., Gordeyev, S., "Atmospheric Propagation v. Aero-Optics", Reno, NV, AIAA 2008-1076, 2008.
15. Fried, D., ”Optical Heterodyne Detection of an Atmospherically Distorted Signal Wave Front,” Proceedings of IEEE, Vol. 55, No. 1, Jan. 1967.
16. APS Study Group Participants and Council Review Committee, ”Report to The American Physical Society of the Study Group on Science and Technology of Directed Energy Weapons,” American Physical Society, Reviews of Modern Physics, Vol. 59, No. 3, Part II, July, 1987.
17. Tyson, R.K., Frazier, B.W., ” Field Guide to Adaptive Optics,” SPIE Press, 2012.
18. Tyson, R.K., *Introduction to Adaptive Optics*, Society of Photo-Optical Instrumentation Engineers, 2000.
19. Martin, J.M., Flatté, S.M., ”Intensity images and statistics from numerical simulation of wave propagation in 3-D random media,” J. Opt. Soc. Am. A., Vol. 27, No. 11, June, 1988.

20. Martin, J.M., Flatté, S.M., ”Simulation of point-source scintillation through three-dimensional random media,” J. Opt. Soc. Am. A., Vol. 7, No. 5, May, 1990.
21. Schmidt, J.D., *Numerical Simulation of Optical Wave Propagation,* Chapter 9: Propagation Through Atmospheric Turbulence,SPIE, 2010.
22. Roggemann, M.C., Welsh, B., *Imaging Through Turbulence,* CRC Press, 1996.
23. Kemnetz M., *Analysis of the Aero-Optical Component of Jitter Using the Stitching Method*, University of Notre Dame, PhD dissertation.
24. Kalensky, M., Diskin, Y., Whiteley, M.R., et al, “Turbulence Profiling Using AAOL-BC,” AIAA Sci-Tech, Orlando, FL, January 6-10, 2020, DOI: 10.2514/6.2020-0682.
25. Kalensky, M., Gordeyev, S., Jumper, E.J., ”In-Flight Studies of Aero-Optical Distortions Around AAOL-BC,” AIAA Aviation, Dallas, TX, June 17-21, 2019, DOI: 10.2514/6.2019-3253.